Heliyon 9 (2023) e20848

Contents lists available at ScienceDirect

Heliyon

journal homepage: www.cell.com/heliyon

Energy eigenvalues and finite-temperature magnetization for the improved Scarf II potential in the presence of external magnetic and Aharonov-Bohm flux fields

E.S. Eyube [a,*], P.P. Notani [b], C.A. Onate [c], U. Wadata [d], E. Omugbe [e], B.M. Bitrus [f], S. D. Najoji [g]

[a] Department of Physics, Faculty of Physical Sciences, Modibbo Adama University, P.M.B. 2076, Yola, Adamawa State, Nigeria
[b] Department of Pure and Applied Sciences, Taraba State Polytechnic, Suntai, P.M.B. 1030, Jalingo, Taraba State, Nigeria
[c] Department of Physics, Kogi State University, Anyigba, Nigeria
[d] Department of Physics, School of Sciences, Aminu Saleh College of Education, P.M.B. 044, Azare, Bauchi State, Nigeria
[e] Department of Physics, University of Agriculture and Environmental Sciences, Umuagwo, P.M.B. 1038, Imo State, Nigeria
[f] Department of Physics, Faculty of Science, Taraba State University, P.M.B. 1176, Jalingo, Taraba State, Nigeria
[g] Department of Science Laboratory Technology, School of Science and Technology, The Federal Polytechnic, P.M.B. 1006, Damaturu, Yobe State, Nigeria

ARTICLE INFO

Keywords:
Magnetization
Diatomic molecules
Energy levels
Magnetic susceptibility
Vector potential
Thermodynamic function

ABSTRACT

In this paper, the bound state solutions of the radial Schrödinger equation are obtained in closed form under an improved Scarf II potential energy function (ISPEF) constrained by external magnetic and Aharonov-Bohm (AB) flux fields. By constructing a suitable Pekeris-like approximation scheme for the centrifugal barrier, approximate analytical expressions for the bound-states and thermal partition function were obtained. With the aid of the partition function, an explicit equation for magnetization at finite temperatures is developed. The obtained equations were then applied to calculate the energy levels and magnetic properties of $^{7}Li_2$ ($2\ ^{3}\Pi_g$), K_2 ($X\ ^{1}\Sigma_g^+$), Mg_2 ($X\ ^{1}\Sigma_g^+$) and NaBr ($X\ ^{1}\Sigma^+$) diatomic molecules. The obtained numerical results of the vibrational energies for these molecules were found to be in good agreement with theoretic and experimental values reported in the existing literature. The results indicated that by turning off the magnetic and AB fields, the energy levels of the diatomic molecules degenerate. The results further revealed that an increase in the temperature of the molecules and the AB field strengths leads to a linear decrease in magnetization.

1. Introduction

A potential function can be regarded as the dependence of the function of a quantum mechanical system on independent parameters such as radial and angular distances. The potential function serves as the medium of interaction between a quantum system and its neighbourhood. Some examples of atomic potential energy models are given elsewhere [1–5]. Diatomic potential energy

* Corresponding author.
E-mail addresses: edwineyubes@mau.edu.ng (E.S. Eyube), ppnotani@gmail.com (P.P. Notani), oaclems14@physicist.net (C.A. Onate), umarwadata72@gmail.com (U. Wadata), omugbeekwevugbe@gmail.com (E. Omugbe), bitrusbako10@yahoo.com (B.M. Bitrus), najojis@gmail.com (S.D. Najoji).

https://doi.org/10.1016/j.heliyon.2023.e20848
Received 5 June 2023; Received in revised form 6 October 2023; Accepted 9 October 2023
Available online 10 October 2023

functions (also known as diatomic oscillators) are specialized potential energy models suitable for the description of interactions in diatomic systems. An essential feature of a molecular interaction potential is that it must obey the three necessary Varshni conditions for a molecular interaction potential [6]. Examples of diatomic molecule potentials are listed in Refs. [7–15].

Diatomic oscillators and atomic potential energy functions are important in the subject of molecular spectroscopy and quantum mechanics due to the information they provide about the quantum states of atoms and molecules of interest. For instance, by solving the wave equation within the non-relativistic and relativistic regimes, under potential functions, many physical properties of systems such as optical, magnetic, electrical, thermodynamic and thermo-chemical properties among others have been investigated [9,16–28].

Several algebraic methods have been constructed to analytically solve the wave equations. Some of the proposed methods include; the functional analysis approach, supersymmetric quantum mechanics approach, Laplace transform method, asymptotic iteration method and so on. Utilizing these methods, the exact and approximate analytical solutions of the Schrödinger equation (SE) have been obtained using different potential functions based on the Pekeris and Greene-Aldrich approximation schemes [29–38].

Researchers have focused a lot of emphasis on the Schrödinger equation bound state solutions under magnetic vector potential fields. The energy spectra have been obtained with the Morse potential, Kratzer potential, screened Coulomb potential, exponential screened Coulomb potentials, and Pöschl-Teller potential, among others, using approximation schemes for the centrifugal barrier [39–42]. Also, the non-relativistic energy levels were obtained with a screened cosine Kratzer potential constrained by external magnetic and AB flux fields [43]. The energy was then applied to derive the partition function and the associated thermodynamic functions.

In earlier works, approximate analytical bound state equations of the SE were obtained with various potential models under external fields. The equations were derived using the Greene-Aldrich approximation which, is restricted to some potential functions and is also not compatible with many others.

Additionally, it has been shown in the literature [15,44,45] that the Greene-Aldrich approximation is a less precise model than the Pekeris approximation scheme for the approximate solution of the SE. In a recent development, several scientists used a Pekeris-type approximation approach to get an approximate analytical solution to the SE under magnetic and AB fields with different potential models [46–48].

In this work, the improved Scarf II potential energy function (ISPEF) is considered. The ISPEF is a member of the class of hyperbolical-type potentials which has practical implications in many fields of Physics [49]. The equation for pure vibrational state energies obtained for the ISPEF has been used to analyze the energy states of diatomic molecules [11]. Thermo-chemical equations of substances have also been reported with various formulations of the ISPEF [8,50].

Motivated by the highly accurate energy eigenvalues obtained with a Pekeris-type approximation scheme [15,44–47], we are encouraged to calculate the energy eigenvalues and finite-temperature magnetization for the improved Scarf II potential perturbed by external magnetic and AB flux fields. To the best of our knowledge, no previous versions of this work have been published in the literature. The remaining parts of the article are organized as follows: In section 2, an approximate energy spectrum would be obtained. Finite-temperature magnetic susceptibility is derived in section 2. Section 3 presents the results and discussion. The paper is concluded in section 4.

2. Bound state solutions of the ISPEF under external magnetic and AB flux fields

In this section, we present the bound state solutions of the SE under the ISPEF. To describe the potential energy-distance relationship in a chemical bond, we utilized the ISPEF model given in Ref. [11].

$$\mathrm{U}(r) = D_{\mathrm{e}} + \frac{U_1 + U_2 \sinh(\alpha r)}{\cosh^2(\alpha r)}, \alpha = \pi c \omega_{\mathrm{e}} (2m_0/D_{\mathrm{e}})^{\frac{1}{2}}, \tag{1}$$

where $U_1 = D_{\mathrm{e}}(\sinh^2 a - 1) U_2 = -2D_{\mathrm{e}} \sinh a$, $a = \alpha r_{\mathrm{e}}$, D_{e} is the equilibrium dissociation energy, r, r_{e} and α is the bond length, and equilibrium bond length and potential screening parameter, respectively. m_0 is the reduced mass, c is the speed of light and ω_{e} is the equilibrium vibrational frequency. The SE for a charged particle under a radial potential, U (r) is given as [30,46]

$$\left\{ \frac{1}{2m_0} \left(-\mathrm{i}\hbar\nabla + \frac{e}{c}\mathbf{A} \right)^2 + \mathrm{U}(r) \right\} \psi(\mathrm{q_i}) = E\, \psi(\mathrm{q_i}), \tag{2}$$

where $\hbar = h/2\pi$, h represents the Planck constant. $\mathrm{q_i}$, E and ψ are the space coordinate, energy and wave function, respectively. **A** is the vector potential, ∇ is a gradient operator, and e denotes the charge. Equation (2) may be rewritten as

$$\left\{ \nabla^2 + \frac{ie}{c\hbar}(\mathbf{A}\cdot\nabla + \nabla\cdot\mathbf{A}) - \frac{e^2\mathbf{A}^2}{c^2\hbar^2} + \frac{2m_0}{\hbar^2}(E - \mathrm{U}) \right\} \psi(\mathrm{q_i}) = 0, \tag{3}$$

The next important task is to choose the vector potential to solve equation (3). It is usual to choose the vector potential so that [40,42].

$$\nabla \times \mathbf{A} = \mathbf{B}, \tag{4}$$

where **B** is the magnetic field vector. Based on the symmetry gauge representation, the vector potential **A** is resolvable into components written as [42]

$$\mathbf{A} = \mathbf{A_1} + \mathbf{A_2}. \tag{5}$$

By putting equation (5) into (4), it is clear that the vectors $\mathbf{A_1}$ and $\mathbf{A_2}$ are constrained by

$$\nabla \times \mathbf{A_1} + \nabla \times \mathbf{A_2} = \mathbf{B}, \tag{6}$$

In accordance with the potential energy function employed in this study, the potential $\mathbf{A_1}$ is taken as $\mathbf{A}_1 = \frac{1}{2}B\tanh(\alpha r)\widehat{\boldsymbol{\varphi}}$, where B is a constant scalar in units of magnetic field strength. Similar vector potential had been applied to study the thermo-magnetic properties of diatomic systems confined by modified Pöschl-Teller potential [41]. By this choice, it is obvious that for values of r of the order of r_e, Taylor series expansion about $r = 0$ gives $\tanh(\alpha r) \approx \alpha r$. Using this approximation, and assuming a cylindrical coordinate system, we have $\nabla \times \mathbf{A_1} \approx \alpha B\widehat{\mathbf{z}}$, where $\widehat{\mathbf{z}}$ represents a unit vector pointing in the z-direction. Following Ref. [42], we let $\mathbf{A_2} = \frac{\Phi_{AB}}{2\pi r}\widehat{\boldsymbol{\varphi}}$, where $\widehat{\boldsymbol{\varphi}}$ is a unit vector in the azimuthal direction, Φ_{AB} denotes the additional magnetic field created by a solenoid [51]. Evidently, it is clear that $\nabla \times \mathbf{A_2} = 0$. Substituting $\nabla \times \mathbf{A_1} \approx \alpha B\widehat{\mathbf{z}}$ and $\nabla \times \mathbf{A_2} = 0$ into expression (6) gives $\mathbf{B} = \alpha B\widehat{\mathbf{z}}$. This result is a demonstration that the magnetic field is of uniform magnitude, $B_0 = \alpha B$ acting in the $\widehat{\mathbf{z}}$. The explicit equation for the magnetic vector potential can be obtained by replacing $\mathbf{A}_1 = \frac{1}{2}B\tanh(\alpha r)\widehat{\boldsymbol{\varphi}}$ and $\mathbf{A_2} = \frac{\Phi_{AB}}{2\pi r}\widehat{\boldsymbol{\varphi}}$ into (5) to yield $\mathbf{A} = \lambda(r)\widehat{\boldsymbol{\varphi}}$, where

$$\lambda(r) = B\tanh(\alpha r) + \frac{\Phi_{AB}}{2\pi r}. \tag{7}$$

Expression (3) and the vector potential $\mathbf{A} = \lambda(r)\widehat{\boldsymbol{\varphi}}$ gives

$$\left\{\frac{\partial^2}{\partial r^2} + \frac{1}{r}\frac{\partial}{\partial r} + \frac{1}{r^2}\frac{\partial^2}{\partial \varphi^2} + \frac{\partial^2}{\partial z^2} + \frac{ie}{c\hbar}\frac{\lambda(r)}{r}\frac{\partial}{\partial \varphi} - \frac{e^2}{c^2\hbar^2}\lambda^2(r) + \frac{2m_0}{\hbar^2}(E - U)\right\}\psi(r,\varphi,z) = 0. \tag{8}$$

Since U (r) and λ (r) are functions of r only, one can focus on the radial component of equation (8) by employing the separation of variables approach. In this approach, an ansatz of the form $\psi(r,\varphi,z) = (2\pi r)^{-\frac{1}{2}}e^{im\varphi}u_{nm}(r)f_{nm}(z)$ is assumed with u_{nm} (r) as the radial wave function. The principal quantum number is given by $n = 0, 1, 2, \ldots$, $m = 0, \pm1, \pm2, \ldots \pm\ell$ is the magnetic quantum number, $\ell = 0, 1, 2, \ldots$is the orbital quantum number and f_n (z) is a function of z [40]. For reason of simplicity, the function f_n (z) is assumed constant in a 2D plane containing the magnetic and AB fields. By inserting the ansatz into equation (8), one obtains

$$u''_{nm}(r) + \left\{\frac{2m_0}{\hbar^2}(E_{nm} - U) - \frac{em}{\hbar c}\frac{\lambda(r)}{r} - \frac{e^2}{\hbar^2c^2}\lambda^2(r) - \frac{m^2 - \frac{1}{4}}{r^2}\right\}u_{nm}(r) = 0, \tag{9}$$

where prime denotes the derivative with respect to r. Using equations (1) and (7) to eliminate U and λ in expression (9) gives

$$u''_{nm}(r) + \frac{2m_0}{\hbar^2}\left\{\begin{array}{l} E_{nm} - D_e - \dfrac{U_1 + U_2\sinh(\alpha r)}{\cosh^2(\alpha r)} \\ -\dfrac{e^2B^2}{2m_0c^2}\tanh^2(\alpha r) - p\dfrac{\tanh(\alpha r)}{r} - q\dfrac{1}{r^2}\end{array}\right\}u_{nm}(r) = 0. \tag{10}$$

where

$$p = \frac{e\hbar B}{2m_0c}\left(m + \frac{e\Phi_{AB}}{\pi\hbar c}\right), q = \frac{\hbar^2}{8m_0}\left\{\left(m + \frac{e\Phi_{AB}}{\pi\hbar c}\right)^2 + 3m^2 - 1\right\}. \tag{11}$$

Due to the presence of $\tanh(\alpha r)/r$ and $1/r^2$, equation (11) can only be solved numerically. Nevertheless, an approximate solution could be obtained by using a Pekeris-type approximation. This model is based on the Taylor series expansion procedure [52,53]. Therefore, for small values of r, the Pekeris approximations to $p\tanh(\alpha r)/r$ and q/r^2 can be written in the form of the potential (1) as

$$p\frac{\tanh(\alpha r)}{r} \approx p\left\{c_0 + \frac{c_1 + c_2\sinh(\alpha r)}{\cosh^2(\alpha r)}\right\}, \tag{12}$$

$$q\frac{1}{r^2} \approx q\left\{d_0 + \frac{d_1 + d_2\sinh(\alpha r)}{\cosh^2(\alpha r)}\right\}. \tag{13}$$

where c_j and b_j ($j = 0, 1, 2$) are given in Appendix A by equations (A12) and (A17), respectively. It follows that by inserting equations (12) and (13) into (10), one obtains

$$u''_{nm}(r) + \frac{2m_0}{\hbar^2}\left\{\begin{array}{l} E_{nm} - D_e - pc_0 - qd_0 - \dfrac{e^2B^2}{2m_0c^2} \\ -\dfrac{U_1 + pc_1 + qd_1 - \dfrac{e^2B^2}{2m_0c^2} + (U_2 + pc_2 + qd_2)\sinh(\alpha r)}{\cosh^2(\alpha r)}\end{array}\right\}u_{nm}(r) = 0, \tag{14}$$

Using the coordinate transformation $z = \mathrm{i}\sinh(\alpha r)$, equation (14) takes the form

$$\left(1-z^2\right)\mathrm{u}_{nm}^{''}(z) - z\mathrm{u}_{nm}^{'}(z) + \left\{a_0 - \frac{\frac{1}{2}(a_1 - \mathrm{i}a_2)}{1-z} - \frac{\frac{1}{2}(a_1 + \mathrm{i}a_2)}{1+z}\right\}\mathrm{u}_{nm}(z) = 0, \tag{15}$$

where

$$\begin{aligned} a_0 &= \frac{2m_0}{\alpha^2\hbar^2}(D_e - E_{nm} + pc_0 + qd_0) + \frac{e^2B^2}{\alpha^2\hbar^2c^2} \\ a_1 &= -\frac{2m_0}{\alpha^2\hbar^2}(U_1 + pc_1 + qd_1) + \frac{e^2B^2}{\alpha^2\hbar^2c^2} \\ a_2 &= -\frac{2m_0}{\alpha^2\hbar^2}(U_2 + pc_2 + qd_2) \end{aligned} \quad . \tag{16}$$

In equation (15), singularities occur at $z = \pm 1$, for this reason, the wave function is assumed as $\mathrm{u}_{nm}(z) = N_{nm}(1-z)^{\frac{1}{2}\sigma}(1+z)^{\frac{1}{2}\tau}\Omega_{nm}(z)$, where σ and τ are constants, N_{nm} is the normalization factor and $\Omega_{nm}(z)$ is a function of z. By inserting this wave function into (15), one obtains

$$\begin{aligned} &\left(1-z^2\right)\Omega_{nm}^{''} + \{\sigma - \tau - (\sigma+\tau+1)z\}\Omega_{nm}^{'} \\ &-\left\{\frac{1}{4}(\sigma+\tau)^2 - a_0 - \frac{\frac{1}{2}(\sigma^2 - \sigma - a_1 + \mathrm{i}a_2)}{1-z} - \frac{\frac{1}{2}(\tau^2 - \tau - a_1 - \mathrm{i}a_2)}{1+z}\right\}\Omega_{nm} = 0. \end{aligned} \tag{17}$$

Equation (17) is Gauss-hypergeometric if the last two terms separately vanish, leading to

$$\sigma = \frac{1}{2} \pm \sqrt{a_1 + \frac{1}{4} - \mathrm{i}a_2}, \tau = \frac{1}{2} \pm \sqrt{a_1 + \frac{1}{4} + \mathrm{i}a_2}. \tag{18}$$

Using the conditions (18), the solution of equation (17) is written as

$$\begin{aligned} \Omega_{nm}(z) &= N_{1m}\,(1-z)^{\frac{1}{2}^{\sigma}}(1+z)^{\frac{1}{2}^{\tau}}{}_2\mathrm{F}_1(a,b;\ c;\ z) \\ &+N_{2m}\,(1-z)^{-\sigma+\frac{1}{2}}(1+z)^{\frac{1}{2}^{\tau}}{}_2\mathrm{F}_1(a+1-c,b+1-c;\ 2-c;\ z), \end{aligned} \tag{19}$$

where N_{1m} and N_{2m} denote the normalization constants, the parameters a, b, and c are given as

$$a = \frac{1}{2}\sigma + \frac{1}{2}\tau + \sqrt{a_0}, b = \frac{1}{2}\sigma + \frac{1}{2}\tau - \sqrt{a_0}, c = \sigma - \tau, \tag{20}$$

For bound-state solution, expression (19) is expected to diverge as $z \to -1$ ($r \to 0$) and must be identically be zero as $z \to 1$ ($r \to \infty$). This means that to obtain a finite wave function when $\sigma > 0$, for $z \to -1$, then $N_{2m} = 0$. Additionally, taking the asymptotic behavior of the Gauss hypergeometric equation into consideration, for the case $z \to 1$, if $\tau > 0$, either a or b must be a negative integer. Letting $b = -n$, equations (16), (18) and (20) yield

$$E_{nm} = D_e + pc_0 + qd_0 + \frac{e^2B^2}{2m_0c^2} - \frac{\alpha^2\hbar^2}{2m_0}\left\{n + \frac{1}{2} - \sqrt{\frac{1}{2}a_1 + \frac{1}{8} + \sqrt{\left(\frac{1}{2}a_1 + \frac{1}{8}\right)^2 + \left(\frac{1}{2}a_2\right)^2}}\right\}^2. \tag{21}$$

if m is given, E_{nm} is expected to increase as n is increased from zero. The maximum vibrational quantum number ($n_{\max}$), can be obtained from the relation $E_{nm}^{'}(n_{\max}) = 0$,

$$n_{\max} = -\frac{1}{2} + \sqrt{\frac{1}{2}a_1 + \frac{1}{8} + \sqrt{\left(\frac{1}{2}a_1 + \frac{1}{8}\right)^2 + \left(\frac{1}{2}a_2\right)^2}}. \tag{22}$$

This implies that the principal quantum number can take values from 0, 1, 2, …, [$n_{\max}$]. The term [$n_{\max}$] signifies the largest integer inferior to $n_{\max}$ if the result computed from expression (21) is not an integer.

3. Magnetization at finite-temperature

Having obtained the energy spectra equation, we proceed to derive the equation for magnetization at finite temperature for the ISPEF. At a temperature, $T \neq 0$, the magnetization is evaluated from the equation [54].

$$\mathrm{M}_m = \frac{1}{\beta}\frac{\partial}{\partial B}\ln \mathrm{Z}, \tag{23}$$

where $\beta = (\mathrm{k_B}T)^{-1}$, $\mathrm{k_B}$ is the Boltzmann constant, Z is the vibrational partition function. The first derivatives of the functions p, q, a_1, a_2 and $n_{\max}$ required for the evaluation of the magnetization are deduced by differentiating equations (11) and (16) with respect to B to obtain

$$p' = \frac{p}{B}, q' = 0, a_1' = \frac{2e^2B}{\alpha^2\hbar^2c^2}\left(1 - \frac{m_0c^2c_1p}{e^2B^2}\right), a_2' = -\frac{2m_0c_2p}{\alpha^2\hbar^2B}, \tag{24}$$

where prime stands for the derivative with respect to B. Expression (22) is also rewritten as

$$\left(n_{\max} + \frac{1}{2}\right)^4 - \left(a_1 + \frac{1}{4}\right)\left(n_{\max} + \frac{1}{2}\right)^2 = \frac{1}{4}a_2^2. \tag{25}$$

Differentiating (25) with respect to B and using (24) to eliminate a_1' and a_2' gives

$$n_{\max}' = \frac{\frac{e^2B}{2\alpha^2\hbar^2c^2}\left(1 - \frac{m_0c^2c_1p}{e^2B^2}\right)\left(n_{\max} + \frac{1}{2}\right)^2 - \frac{m_0a_2c_2p}{4\alpha^2\hbar^2B}}{\left(n_{\max} + \frac{1}{2}\right)^3 - \frac{1}{2}\left(a_1 + \frac{1}{4}\right)\left(n_{\max} + \frac{1}{2}\right)}. \tag{26}$$

The vibrational partition function is given by the equation [18].

$$\mathrm{Z} = \sum_{n=0}^{n_{\max}} \mathrm{e}^{-\beta E_{nm}}. \tag{27}$$

Inserting equation (21) into (27), with the help of (22), we obtain

$$\mathrm{Z} = \mathrm{Z}_0 \sum_{n=0}^{n_{\max}} \mathrm{F}(n), \tag{28}$$

where

$$\mathrm{Z}_0 = \exp\left(-\beta D_e - \beta p c_0 - \beta q d_0 - \frac{\beta e^2B^2}{2m_0c^2}\right), \varepsilon = \alpha\hbar\sqrt{\frac{\beta}{2m_0}}, \mathrm{F}(n) = \exp\left(\varepsilon n - \varepsilon n_{\max}\right)^2, \tag{29}$$

The summation in (28) can be obtained approximately with the aid of the modified Poisson summation formula [55]. By employing the result given by equation (36) of Ref. [50], the lowest order approximation for the summation in (28) is obtained as

$$\sum_{n=0}^{n_{\max}} \mathrm{F}(n) = \frac{1}{2}\left\{\exp\left(\varepsilon^2 n_{\max}^2\right) - \exp\left(\varepsilon^2\right)\right\} + \frac{\sqrt{\pi}}{2\varepsilon}\left\{\mathrm{Erfi}(\varepsilon n_{\max}) + \mathrm{Erfi}(\varepsilon)\right\}, \tag{30}$$

where Erfi denotes the imaginary error function. Inserting equation (30) into (28), the partition function is found as

$$\mathrm{Z} = \frac{1}{2}\mathrm{Z}_0\left\{\exp\left(\varepsilon^2 n_{\max}^2\right) - \exp\left(\varepsilon^2\right) + \frac{\sqrt{\pi}}{\varepsilon}\left[\mathrm{Erfi}(\varepsilon n_{\max}) + \mathrm{Erfi}(\varepsilon)\right]\right\}. \tag{31}$$

Substituting equation (31) into (23) gives

$$\mathrm{M}_m = -\left(p' c_0 + q' d_0 + \frac{e^2B}{m_0c^2}\right) + \frac{\mathrm{Z}_0}{\beta Z} n_{\max}'\left(\varepsilon^2 n_{\max} + 1\right)\exp\left(\varepsilon^2 n_{\max}^2\right). \tag{32}$$

Using equations (24) and (26) to eliminate the first derivatives in (32), the finite-temperature magnetization formula is obtained as

$$\mathrm{M}_m = -\frac{pc_0}{B} - \frac{e^2B}{m_0c^2} + \frac{\mathrm{Z}_0}{\beta Z}\frac{\left\{\frac{e^2B}{2\alpha^2\hbar^2c^2}\left(1 - \frac{m_0c^2c_1p}{e^2B^2}\right)\left(n_{\max} + \frac{1}{2}\right)^2 - \frac{m_0a_2c_2p}{4\alpha^2\hbar^2B}\right\}\left(\varepsilon^2 n_{\max} + 1\right)\exp\left(\varepsilon^2 n_{\max}^2\right)}{\left(n_{\max} + \frac{1}{2}\right)^3 - \frac{1}{2}\left(a_1 + \frac{1}{4}\right)\left(n_{\max} + \frac{1}{2}\right)}. \tag{33}$$

4. Results and discussion

The equations of the energy levels and magnetization are applied to diatomic substances including $^7Li_2$ ($2\,^3\Pi_g$), K_2 ($X\,^1\Sigma_g^+$), Mg_2 (X

$^1\Sigma_g^+$) and NaBr ($X\ ^1\Sigma^+$) molecules. The diatomic molecules are chosen based on the availability of experimental data for spectroscopic constants and vibrational energies. The spectroscopic constants are listed in Table 1. The observed values of D_e, r_e and ω_e given in the table were those reported in the literature [56–59]. The results in the last column of the table are obtained with the expression for the potential screening parameter given in (1).

First and foremost, we confirm the validity of the approximation schemes (12) and (13) used in the study. In Figs. 1–4, the function $X_1 = pr^{-1}\tanh(\alpha r)$ and the approximation model $X_2 = pc_0 + p[c_1 + c_2\sinh(\alpha r)]\mathrm{sech}^2(\alpha r)$ are plotted as function of internuclear separation r for the diatomic molecules. The graphical plots in Figs. 5–8 are obtained with $Y_1 = qr^{-2}$ and the approximation function $Y_2 = qd_0 + q[d_1 + d_2\sinh(\alpha r)]\mathrm{sech}^2(\alpha r)$. Evidently, the figures reveal that for the small values of the internuclear separations used, the data calculated with X_2 and Y_2 are in agreement those obtained with X_1 and Y_1, respectively. The results signify that the Pekeris approximation schemes (12) and (13) may be applied to obtain the approximate solution of the radial SE given by equation (10).

It is worthy to relate the present results with the literature on ISPEF. In Ref. [11], the equation for the energy spectra was obtained at zero external fields. In contrast, the equation for the energy levels obtained in the present work depends on the external magnetic and AB fields. In addition, the radial SE (13) of Ref. [11] was derived based on transformations involving spherical coordinates. However, in this work, transformation equation in cylindrical coordinates was used to obtain the Schrödinger equation. Therefore, when the external magnetic and AB fields are not present, it will be appropriate to compare the equations obtained in this study with those given in Ref. [11].

Letting $B = \Phi_{AB} = 0$, equation (11) gives $p = 0$ and $q = \frac{\hbar^2}{2m_0}\left(m^2 - \frac{1}{4}\right)$. These results inserted in equation (10) yields

$$\mathrm{u}_n^{''}(r) + \frac{2\mathrm{M}_0}{\hbar^2}\left\{E_{nm} - \mathrm{U}(r) - \frac{\hbar^2\left(m^2 - \frac{1}{4}\right)}{2\mathrm{M}_0 r^2}\right\}\mathrm{u}_n(r) = 0. \tag{34}$$

Equation (34) is the same to equation (13) of Ref. [11] if $m = \ell + ½$. This means that the substitution $m = \ell + ½$ converts equations in 2D to equations in 3D. Conversely, $\ell = |m| - \frac{1}{2}$ changes equations in 3D to equations in 2D. Using $B = \Phi_{AB} = 0$, the relation $m = \ell + ½$, and the mapping $D_e \to \eta D_e$, equation (21) reproduces expression (50) of Ref. [11].

With the aid of expression (21), the energy is generated for the diatomic molecules with $B = \Phi_{AB} = m = 0$. The data are given in Table 2 and Table 3. The results show that the energy levels of the increase as n increases up to the maximum vibrational quantum number. Equation (22) gives n_{max} as 89, 96, 16 and 186 for the $^7Li_2$ ($2\ ^3\Pi_g$). K_2 ($X\ ^1\Sigma_g^+$), Mg_2 ($X\ ^1\Sigma_g^+$) and NaBr ($X\ ^1\Sigma^+$) molecules, respectively. Equation (50) of Ref. [11] has also been used to calculate the vibrational quantum state ($\ell = 0$) energies (E_n) for the molecules. The results obtained as well as the literature on the vibrational energies of diatomic molecules are given in Tables 2 and 3. Using the experimental data as the standard for comparison, it is obvious that the results obtained with the present model are better compared to the energy eigenvalues calculated by using equation (50) of Ref. [11].

The variations of the energy with both the magnetic field and AB flux fields are also examined for the molecules. Table 4 and Table 5 shows the results of numerical computations using equation (21). The computed results are obtained with and without external magnetic and AB fields. The computations are carried out at arbitrary values of n and m. As shown in the tables, with the external fields set to zero ($B = \Phi_{AB} = 0$), and constant n, the energy spectra for $m = \pm\ell$ are indistinguishable which is an indication of degenerate energy levels in the diatomic molecules.

By including only one of the external fields and excluding the other, the tabulated results show that, irrespective of the external field present, if m is fixed, the energy eigenvalue of a molecule increases with an increase in B or Φ_{AB} relative to the energy of the system without the external fields. Fig. 9 shows the variations in the energy with n obtained for different values of Φ_{AB}. In Fig. 10, the energy spectra are plotted against n for different values of B. The data in the figures are obtained with the parameters of the $^7Li_2$ ($2\ ^3\Pi_g$) molecule. Similar plots were obtained with the parameters of K_2 ($X\ ^1\Sigma_g^+$), Mg_2 ($X\ ^1\Sigma_g^+$) and NaBr ($X\ ^1\Sigma^+$) molecules. The plots reveal that AB fields of the order of just a few militesla are sufficient to remove degeneracy from the system. Nevertheless, under a magnetic field, values of B in the range of megatesla are needed to lift the energy overlap of the molecules. For this purpose, a laser pulse implosion device (LPID) could be employed. The LPID is known to produce very strong magnetic fields of the order of thousands megatesla [60]. If the external fields are both turned on ($B \neq 0$, $\Phi_{AB} \neq 0$), the energy eigenvalues of the molecules are summarized in Tables 4 and 5. The results reveal that at a given value of m, the energy of a molecule is increased, in addition, degeneracy in the energy levels is completely eliminated, leading to a more bounded system.

Figs. 11–13 show the variation of the magnetization as a function of; magnetic quantum number, magnetic field, and AB field at

Table 1
Spectroscopic parameters of the diatomic molecules investigated in this study.

Molecule	State	Spectroscopic parameter			Ref.	α (Å^{-1})
		D_e (cm^{-1})	r_e (Å)	ω_e (cm^{-1})		
$^7Li_2$	$2\ ^3\Pi_g$	8479.621	3.8463419	188.6858	[56]	0.4674
K_2	$X\ ^1\Sigma_g^+$	4447	3.92433	92.398475	[57]	0.7460
Mg_2	$X\ ^1\Sigma_g^+$	424	3.890	51.121	[58]	1.0540
NaBr	$X\ ^1\Sigma^+$	27270.21	2.359	293.2	[59]	0.9123

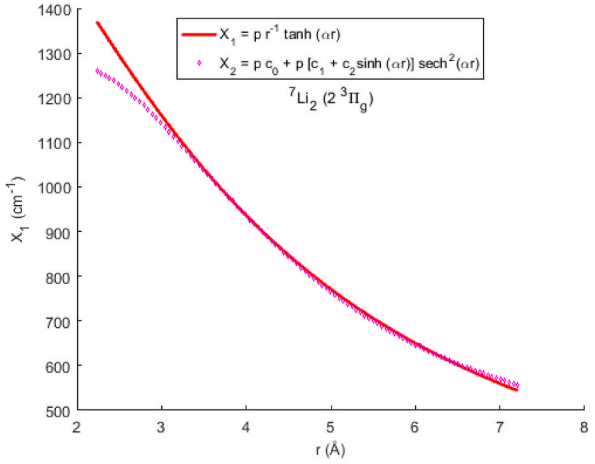

Fig. 1. Fitting of the Pekeris approximation scheme $pc_0 + p[c_1 + c_2 \sinh(\alpha r)]\mathrm{sech}^2(\alpha r)$ to the function $pr^{-1}\tanh(\alpha r)$ for the Li_2 ($2\ ^3\Pi_g$) molecule.

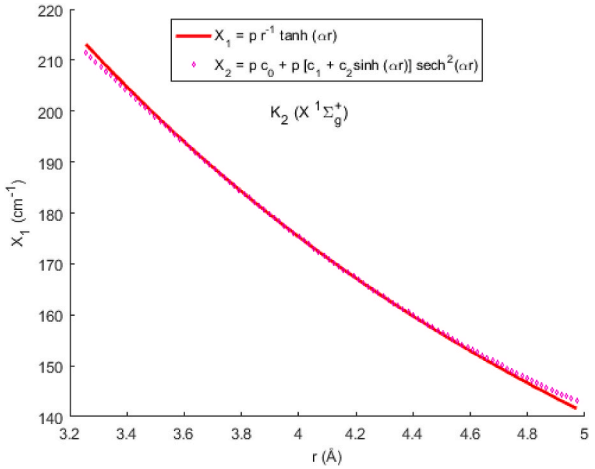

Fig. 2. Fitting of the Pekeris approximation scheme $pc_0 + p[c_1 + c_2 \sinh(\alpha r)]\mathrm{sech}^2(\alpha r)$ to the function $pr^{-1}\tanh(\alpha r)$ for the K_2 ($X\ ^1\Sigma_g^+$) molecule.

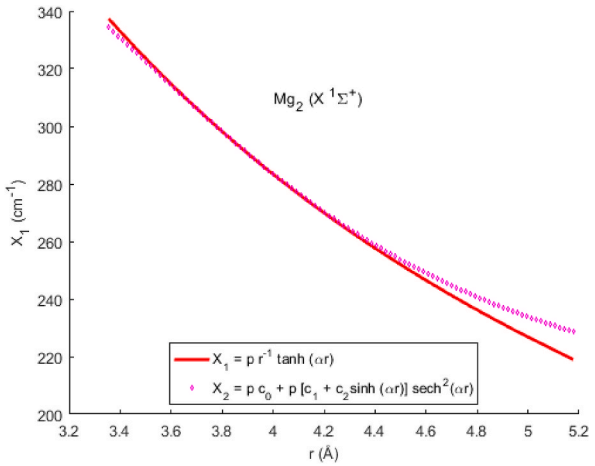

Fig. 3. Fitting of the Pekeris approximation scheme $pc_0 + p[c_1 + c_2 \sinh(\alpha r)]\mathrm{sech}^2(\alpha r)$ to the function $pr^{-1}\tanh(\alpha r)$ for the Mg_2 ($X\ ^1\Sigma^+$) molecule.

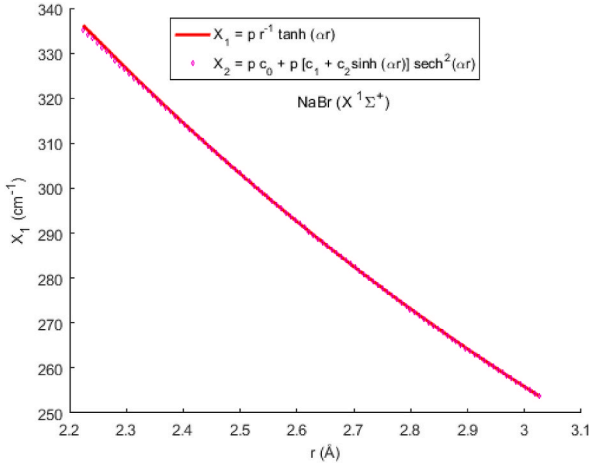

Fig. 4. Fitting of the Pekeris approximation scheme $pc_0 + p[c_1 + c_2 \sinh(\alpha r)]\mathrm{sech}^2(\alpha r)$ to the function $pr^{-1} \tanh(\alpha r)$ for the NaBr ($X\ ^1\Sigma^+$) molecule.

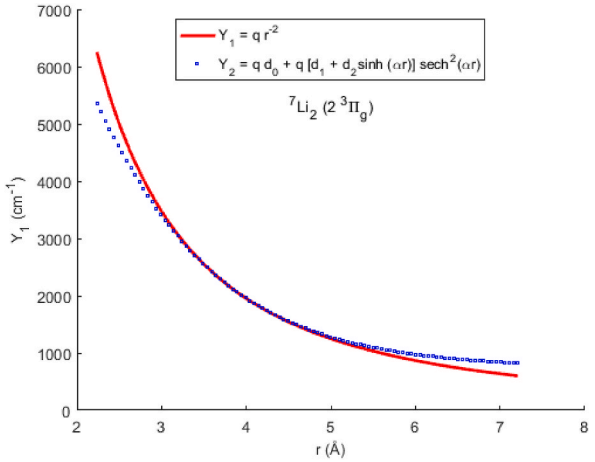

Fig. 5. Fitting of the Pekeris approximation scheme $qd_0 + q[d_1 + d_2 \sinh(\alpha r)]\mathrm{sech}^2(\alpha r)$ to the function qr^{-2} for the Li_2 ($2\ ^3\Pi_g$) molecule.

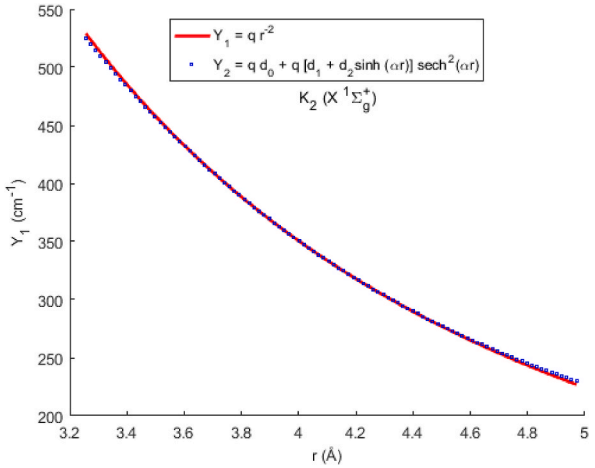

Fig. 6. Fitting of the Pekeris approximation scheme $qd_0 + q[d_1 + d_2 \sinh(\alpha r)]\mathrm{sech}^2(\alpha r)$ to the function qr^{-2} for the K_2 ($X\ ^1\Sigma_g^+$) molecule.

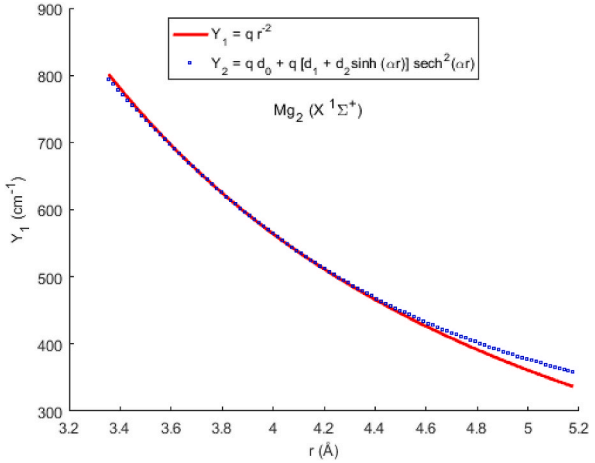

Fig. 7. Fitting of the Pekeris approximation scheme $qd_0 + q[d_1 + d_2\,\sinh(\alpha r)]\mathrm{sech}^2(\alpha r)$ to the function qr^{-2} for the Mg_2 ($X\ ^1\Sigma^+$) molecule.

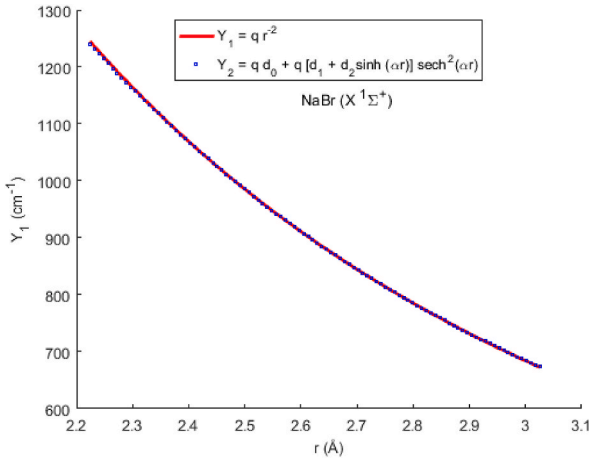

Fig. 8. Fitting of the Pekeris approximation scheme $qd_0 + q[d_1 + d_2\,\sinh(\alpha r)]\mathrm{sech}^2(\alpha r)$ to the function qr^{-2} for the NaBr ($X\ ^1\Sigma^+$) molecule.

Table 2
Vibrational energy (cm^{-1}) for $^7Li_2$ ($2\ ^3\Pi_g$) and K_2 ($X\ ^1\Sigma_g^+$) diatomic molecules ($B = \Phi_{AB} = 0$).

n	$^7Li_2$ ($2\ ^3\Pi_g$)			n	K_2 ($X\ ^1\Sigma_g^+$)		
	E_{n0} (19)	E_{exp} [56]	E_n [11]		E_{n0} (19)	E_{exp} [57]	E_n [11]
0	93.9724	93.8116	94.0533	0	46.064	46.094	46.078
1	280.5599	280.1512	280.6402	1	137.503	137.839	137.516
2	465.0480	464.2410	465.1277	2	227.981	228.927	227.995
3	647.4368	646.1710	647.5159	3	317.500	319.354	317.514
4	827.7264	826.0218	827.8049	4	406.059	409.116	406.073
5	1005.9167	1003.8648	1005.9945	5	493.658	498.209	493.672
6	1182.0076	1179.7632	1182.0849	6	580.297	586.628	580.311
7	1355.9993	1353.7728	1356.0760	7	665.976	674.369	665.990
8	1527.8917	1525.9427	1527.9678	8	750.696	761.427	750.709
9	1697.6848	1696.3158	1697.7603	9	834.455	847.797	834.468
10	1865.3787	1864.9297	1865.4535	10	917.255	933.474	917.267
11	2030.9732	2031.8171	2031.0475	11	999.094	1018.451	999.107
12	2194.4685	2197.0063	2194.5421	12	1079.974	1102.724	1079.986
13	2355.8644	2360.5220	2355.9375	13	1159.893	1186.286	1159.906
14	2515.1611	2522.3854	2515.2336	14	1238.853	1269.131	1238.866
15	2672.3585	2682.6150	2672.4304	15	1316.853	1351.252	1316.866
…	…	…	…	16	1393.893	1432.642	1393.905
41	6022.6405	6299.0486	6022.6967	17	1469.973	1513.294	1469.985

Table 3
Vibrational energy (cm^{-1}) for Mg_2 ($X\ ^1\Sigma^+$) and NaBr ($X\ ^1\Sigma^+$) diatomic molecules ($B = \Phi_{AB} = 0$).

n	Mg_2 ($X\ ^1\Sigma^+$)			n	NaBr ($X\ ^1\Sigma^+$)		
	E_{n0} (19)	E_{exp} [58]	E_n [11]		E_{n0} (19)	E_{exp} [59]	E_n [11]
0	25.152	25.156	25.175	0	146.36	146.31	146.40
1	73.192	73.037	73.214	1	437.98	436.99	438.02
2	118.151	117.757	118.172	2	728.03	725.28	728.07
3	160.027	159.384	160.047	3	1016.50	1011.18	1016.54
4	198.822	197.971	198.841	4	1303.40	1294.71	1303.43
5	234.534	233.558	234.553	5	1588.72	1575.85	1588.75
6	267.166	266.168	267.183	6	1872.46	1854.66	1872.50
7	296.715	295.811	296.732	7	2154.63	2131.14	2154.66
8	323.182	322.484	323.199	8	2435.22	2405.33	2435.25
9	346.568	346.162	346.584	9	2714.23	2677.29	2714.27
10	366.872	366.806	366.887	10	2991.67	2947.14	2991.71
11	384.094	384.393	384.108	11	3267.53	3215.02	3267.57
12	398.234	398.831	398.248	…	…	…	…

Table 4
2D Energy eigenvalues (in eV) for various values of B and Φ_{AB} for the diatomic molecules.

n	m	$^7Li_2$ ($2\ ^3\Pi_g$)				n	m	K_2 ($X\ ^1\Sigma_g^+$)			
		$B = 0$ $\Phi_{AB} = 0$	$B = 0$ $\Phi_{AB} = 0.1$ mT	$B = 100$ kT $\Phi_{AB} = 0$	$B = 100$ kT $\Phi_{AB} = 0.1$ mT			$B = 0$ $\Phi_{AB} = 0$	$B = 0$ $\Phi_{AB} = 0.1$ mT	$B = 100$ kT $\Phi_{AB} = 0$	$B = 100$ kT $\Phi_{AB} = 0.1$ mT
0	0	0.01165	0.25434	1.35913	2.76107	0	0	0.00571	0.05028	0.27716	0.53868
2	−2	0.05782	0.29134	1.39359	2.77418	2	−2	0.02829	0.07115	0.29708	0.55517
	−1	0.05770	0.29400	1.40128	2.78262		−1	0.02827	0.07167	0.29842	0.55698
	0	0.05766	0.29673	1.40906	2.79108		0	0.02827	0.07220	0.29978	0.55881
	1	0.05770	0.29952	1.41693	2.79958		1	0.02827	0.07275	0.30115	0.56064
	2	0.05782	0.30238	1.42488	2.80811		2	0.02829	0.07331	0.30253	0.56249
3	−3	0.08062	0.30960	1.41070	2.78060	3	−3	0.03943	0.08144	0.30690	0.56328
	−2	0.08043	0.31218	1.41825	2.78894		−2	0.03939	0.08194	0.30823	0.56507
	−1	0.08031	0.31483	1.42590	2.79730		−1	0.03937	0.08246	0.30956	0.56688
	0	0.08027	0.31754	1.43363	2.80570		0	0.03937	0.08299	0.31091	0.56869
	1	0.08031	0.32031	1.44145	2.81413		1	0.03937	0.08353	0.31227	0.57052
	2	0.08043	0.32314	1.44936	2.82258		2	0.03939	0.08408	0.31365	0.57236
	3	0.08062	0.32604	1.45736	2.83107		3	0.03943	0.08465	0.31504	0.57421
6	−6	0.14793	0.36345	1.46154	2.79935	6	−6	0.07219	0.11171	0.33580	0.58709
	−5	0.14751	0.36579	1.46870	2.80738		−5	0.07211	0.11216	0.33706	0.58882
	−4	0.14716	0.36818	1.47594	2.81543		−4	0.07205	0.11262	0.33834	0.59056
	−3	0.14690	0.37064	1.48327	2.82352		−3	0.07201	0.11310	0.33963	0.59231
	−2	0.14670	0.37316	1.49069	2.83165		−2	0.07197	0.11359	0.34094	0.59407
	−1	0.14659	0.37574	1.49820	2.83980		−1	0.07195	0.11410	0.34226	0.59585
	0	0.14655	0.37839	1.50579	2.84798		0	0.07195	0.11462	0.34359	0.59763
	1	0.14659	0.38110	1.51347	2.85619		1	0.07195	0.11515	0.34493	0.59943
	2	0.14670	0.38387	1.52124	2.86443		2	0.07197	0.11569	0.34629	0.60124
	3	0.14690	0.38670	1.52909	2.87270		3	0.07201	0.11624	0.34766	0.60306
	4	0.14716	0.38959	1.53702	2.88100		4	0.07205	0.11681	0.34905	0.60489
	5	0.14751	0.39255	1.54504	2.88932		5	0.07211	0.11739	0.35045	0.60673
	6	0.14793	0.39556	1.55314	2.89767		6	0.07219	0.11799	0.35186	0.60859

different temperatures of the $^7Li_2$ ($2\ ^3\Pi_g$) molecule. The plots reveal a decrease in magnetization with increasing m, B or Φ_{AB}. In Fig. 11, it is clear that negative values of m give rise to positive magnetization and vice-versa. Fig. 13 also indicates that if the AB field is kept constant, an increase in the temperature of the molecules leads to an increase in magnetization. Fig. 11 illustrates the concept of antisymmetric magnetization. The magnetic order of the system is paramagnetic if m is negative, and diamagnetic if m is positive. The antisymmetric feature was removed under the external field as shown in Figs. 12 and 13. The negative magnetization indicates a diamagnetic phenomenon since the susceptibility will also be negative. Negative magnetization has many applications in physics such as in magnetic switching and spin resolve devices [61].

5. Conclusions

The radial SE is solved with the ISPEF under external magnetic and AB flux fields. By utilizing the ansatz solution technique, an approximate energy equation is obtained in closed form within the context of the Pekeris-type approximation. The energy equation was used to develop the thermal partition function and magnetization formula for the ISPEF. The equation for the energy eigenvalues is used to obtain numerical vibrational energies for the diatomic molecules including $^7Li_2$ ($2\ ^3\Pi_g$), K_2 ($X\ ^1\Sigma_g^+$), Mg_2 ($X\ ^1\Sigma_g^+$) and NaBr (X

Table 5
2D Energy eigenvalues (in eV) for various values of B and Φ_{AB} for the diatomic molecules.

n	m	Mg_2 ($X\ ^1\Sigma^+$)				n	m	NaBr ($X\ ^1\Sigma^+$)			
		$B=0$ $\Phi_{AB}=0$	$B=0$ $\Phi_{AB}=0.1$ mT	$B=100$ kT $\Phi_{AB}=0$	$B=100$ kT $\Phi_{AB}=0.1$ mT			$B=0$ $\Phi_{AB}=0$	$B=0$ $\Phi_{AB}=0.1$ mT	$B=100$ kT $\Phi_{AB}=0$	$B=100$ kT $\Phi_{AB}=0.1$ mT
0	0	0.00312	0.06895	0.44434	0.72505	0	0	0.01815	0.13561	0.30813	0.79285
2	−2	0.01469	0.07403	0.45168	0.73727	2	−2	0.09034	0.20400	0.37587	0.85503
	−1	0.01466	0.07466	0.45380	0.73717		−1	0.09028	0.20538	0.37810	0.85865
	0	0.01465	0.07531	0.45593	0.73699		0	0.09026	0.20680	0.38037	0.86230
	1	0.01466	0.07598	0.45808	0.73672		1	0.09028	0.20825	0.38268	0.86598
	2	0.01469	0.07665	0.46025	0.73636		2	0.09034	0.20974	0.38502	0.86969
3	−3	0.01993	0.07612	0.45493	0.74224	3	−3	0.12619	0.23797	0.40952	0.88592
	−2	0.01988	0.07671	0.45699	0.74237		−2	0.12610	0.23931	0.41171	0.88948
	−1	0.01985	0.07731	0.45906	0.74242		−1	0.12605	0.24069	0.41394	0.89309
	0	0.01984	0.07792	0.46115	0.74239		0	0.12603	0.24210	0.41620	0.89672
	1	0.01985	0.07855	0.46326	0.74227		1	0.12605	0.24355	0.41850	0.90039
	2	0.01988	0.07919	0.46538	0.74206		2	0.12610	0.24503	0.42083	0.90410
	3	0.01993	0.07984	0.46752	0.74176		3	0.12619	0.24655	0.42321	0.90784
6	−6	0.03344	0.08052	0.46294	0.75278	6	−6	0.23279	0.33898	0.50957	0.97773
	−5	0.03335	0.08099	0.46483	0.75353		−5	0.23260	0.34020	0.51164	0.98116
	−4	0.03327	0.08146	0.46674	0.75421		−4	0.23244	0.34146	0.51374	0.98463
	−3	0.03320	0.08194	0.46866	0.75483		−3	0.23232	0.34275	0.51588	0.98813
	−2	0.03316	0.08244	0.47060	0.75539		−2	0.23223	0.34407	0.51806	0.99166
	−1	0.03313	0.08294	0.47255	0.75588		−1	0.23217	0.34543	0.52027	0.99523
	0	0.03312	0.08346	0.47452	0.75629		0	0.23216	0.34683	0.52251	0.99883
	1	0.03313	0.08399	0.47650	0.75662		1	0.23217	0.34826	0.52479	1.00247
	2	0.03316	0.08452	0.47850	0.75688		2	0.23223	0.34972	0.52711	1.00614
	3	0.03320	0.08507	0.48051	0.75704		3	0.23232	0.35122	0.52946	1.00984
	4	0.03327	0.08562	0.48254	0.75712		4	0.23244	0.35275	0.53185	1.01358
	5	0.03335	0.08619	0.48457	0.75711		5	0.23260	0.35432	0.53427	1.01735
	6	0.03344	0.08676	0.48662	0.75699		6	0.23279	0.35593	0.53673	1.02115

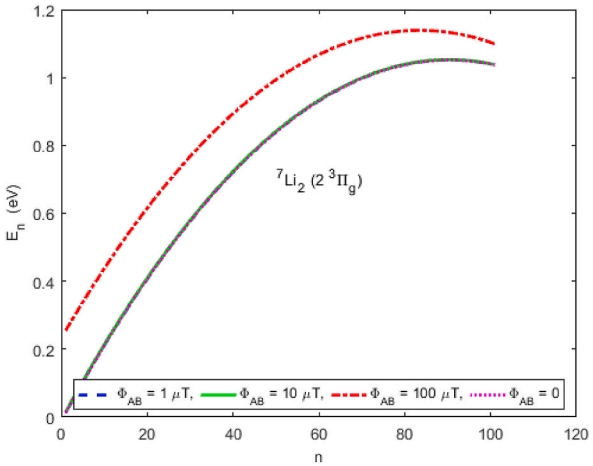

Fig. 9. Graphical representation of the vibrational energy eigenvalues at different values of Φ_{AB} for the $^7Li_2$ ($2\ ^3\Pi_g$) molecule.

$^1\Sigma^+$) molecules. The results were found to be in perfect agreement with theoretical work on the ISPEF and available experimental data. The results showed that when the external fields were turned off ($B=\Phi_{AB}=0$), the energy spectra of the molecules were degenerate. Also, the energy overlap is removed if the external fields are present. The results further indicated that the magnetization increases with increasing temperature of the molecules and decreases with increasing AB field intensity. The equations and numerical data obtained in this research may have practical implications in areas of chemical physics, chemical engineering, atomic and molecular physics, and solid-state physics.

Data availability statement

Data included in article/supplementary material/referenced in article.

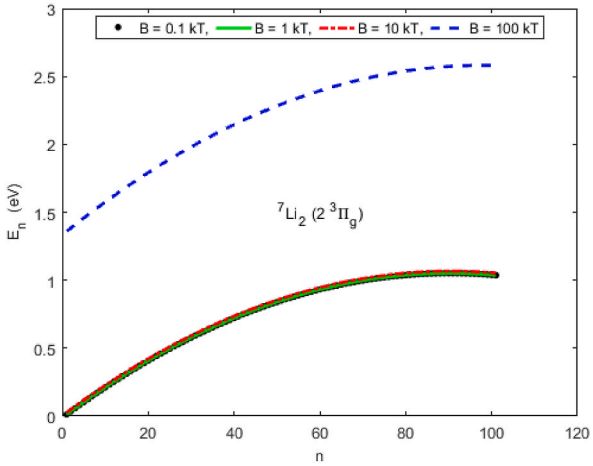

Fig. 10. Graphical representation of the vibrational energy eigenvalues at different values of B for the $^7Li_2$ ($2\ ^3\Pi_g$) molecule.

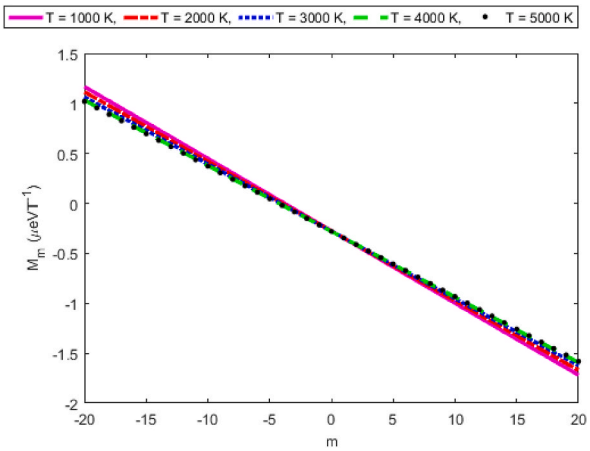

Fig. 11. Variations of magnetization with magnetic quantum number at different temperatures of the $^7Li_2$ ($2\ ^3\Pi_g$) molecule.

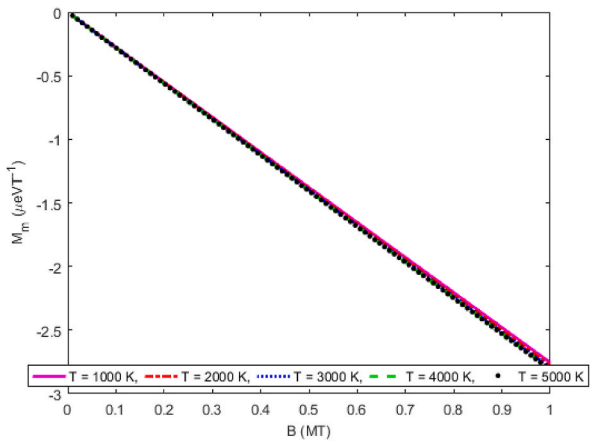

Fig. 12. Variations of magnetization with magnetic field at different temperatures of the $^7Li_2$ ($2\ ^3\Pi_g$) molecule.

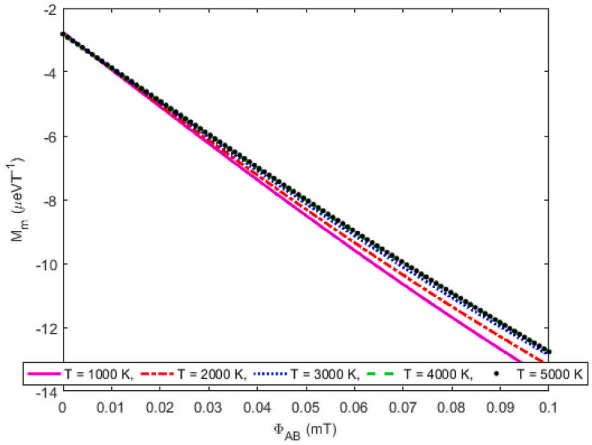

Fig. 13. Variations of magnetization with AB field at different temperatures of the $^7Li_2$ ($2\ ^3\Pi_g$) molecule.

CRediT authorship contribution statement

E.S. Eyube: Writing – review & editing, Writing – original draft, Validation, Supervision, Software, Resources, Project administration, Methodology, Investigation, Formal analysis, Data curation, Conceptualization. **P.P. Notani:** Writing – review & editing, Writing – original draft, Validation, Resources, Methodology, Investigation, Formal analysis, Data curation. **C.A. Onate:** Writing – review & editing, Writing – original draft, Validation, Supervision, Resources, Project administration, Investigation, Formal analysis. **U. Wadata:** Writing – review & editing, Writing – original draft, Validation, Resources, Investigation, Data curation. **E. Omugbe:** Writing – review & editing, Writing – original draft, Visualization, Validation, Software, Resources, Investigation, Formal analysis, Data curation. **B.M. Bitrus:** Writing – review & editing, Writing – original draft, Validation, Resources, Investigation, Formal analysis. **S.D. Najoji:** Writing – review & editing, Writing – original draft, Visualization, Validation, Resources, Formal analysis, Data curation.

Declaration of competing interest

The authors declare that they have no known competing financial interests or personal relationships that could have appeared to influence the work reported in this paper.

Appendix A

This section is devoted to the derivation of the Pekeris approximation schemes used in solving the radial SE (7). The Pekeris approximation is a method of expressing a general function $\chi(r)$ as a linear combination of differentiable and continuous functions $\varphi(r)$ and $\theta(r)$ [47]. By expressing the terms $r^{-1}\tanh(\alpha r)$ and r^{-2} in the same functional form as the potential (1), approximate analytical solution of equation (7) can be obtained. Based on this reason, we write the function $\chi(r)$ in the form

$$\psi(r) \approx A + \frac{B + C\sinh(\alpha r)}{\cosh^2(\alpha r)}, \tag{A1}$$

where $A \equiv (c_0, d_0, \ldots)$, $B \equiv (c_1, d_1, \ldots)$ and $C \equiv (c_2, d_2, \ldots)$ are constant coefficients to be determined by expanding $\chi(r)$ in Taylor series about the point $x = 0$, where $x = r/r_e$ - 1 [46,47]. For different selections of A, B, C, and $\chi(r)$, equations (9) and (10) represent the Pekeris approximation for the functions $r^{-1}\tanh(\alpha r)$ and r^{-2}, respectively. Therefore, in terms of the variable x, equation (A1) is recast in a more convenient form as

$$\chi(x) \approx A + B\varphi(x) + C\theta(x), \tag{A2}$$

where

$$\varphi(x) = \mathrm{sech}^2(ax + a), \tag{A3}$$

$$\theta(x) = \sinh(ax + a)\mathrm{sech}^2(ax + a), a = \alpha r_e. \tag{A4}$$

The Taylor series expansion of expressions (A3) and (A4) about $x = 0$ are obtained as

$$\varphi(x) \approx \varphi_0 - a\varphi_0(2\tanh a)x + a^2\varphi_0\left(3\tanh^2 a - 1\right)x^2 + \cdots, \tag{A5}$$

$$\theta(x) \approx \theta_0 - a\theta_0(2\tanh a - \coth a)x + a^2\theta_0\left(3\tanh^2 a - \frac{5}{2}\right)x^2 + \cdots. \tag{A6}$$

where $\varphi_0 = \operatorname{sech}^2 a$ and $\theta_0 = \operatorname{sech}^2 a \sinh a$. By inserting equations (A5) and (A6) into (A2), one obtains

$$\begin{aligned}\chi(x) \approx{}& A + \varphi_0 B + \theta_0 C - a\{2\varphi_0 B \tanh a + \theta_0 C(2\tanh a - \coth a)\}x \\ &+ a^2\left\{\varphi_0 B\left(3\tanh^2 a - 1\right) + \theta_0 C\left(3\tanh^2 a - \frac{5}{2}\right)\right\}x^2 + \cdots.\end{aligned} \tag{A7}$$

Letting $\chi(r) = r^{-1}\tanh(\alpha r)$ and inserting $r = r_e(1 + x)$, the Taylor series expansion of $\chi(x)$ about the point $x = 0$ yields

$$\chi(x) = \chi_0 - \chi_0\delta x + \chi_0\left(\delta - a^2\operatorname{sech}^2 a\right)x^2 + \ldots, \tag{A8}$$

where $\chi_0 = r_e^{-1}\tanh a$, $\delta = 1 - a\,\operatorname{csch} a \operatorname{sech} a$. Plugging equation (A8) into (A7) and equating corresponding coefficients of x^0, x, x^2 gives

$$c_0 + \varphi_0 c_1 + \theta_0 c_2 = \chi_0, \tag{A9}$$

$$(2\varphi_0 a\tanh a)c_1 + a\theta_0(2\tanh a - \coth a)c_2 = \chi_0\delta, \tag{A10}$$

$$a^2\varphi_0\left(3\tanh^2 a - 1\right)c_1 + a^2\theta_0\left(3\tanh^2 a - \frac{5}{2}\right)c_2 = \chi_0\left(\delta - a^2\operatorname{sech}^2 a\right). \tag{A11}$$

where A, B and C have been replaced with c_0, c_1 and c_2, respectively. Solving equation (A9)- (A11) gives

$$\begin{aligned} c_0 &= \frac{\tanh a\left(7 - \tanh^2 a\right)}{6r_e} - \frac{1}{2ar_e} + \frac{\tanh a}{3a^2 r_e} \\ c_1 &= \frac{\tanh a\left(1 - 2\tanh^2 a\right)}{3r_e} + \frac{\delta(11 - \cosh 2a)}{12ar_e} - \frac{\delta\tanh a(3 - \cosh 2a)}{6a^2 r_e} \\ c_2 &= \frac{2\operatorname{sech} a\tanh^2 a}{3r_e} + \frac{\delta\sinh a\left(3\tanh^2 a - 1\right)}{3ar_e} - \frac{2\delta\sinh a\tanh a}{3a^2 r_e} \end{aligned} \tag{A12}$$

The Pekeris approximation for r^{-2} is deduced by choosing $\chi(r) = r^{-2}$. Putting $r = r_e(1 + x)$ into this expression, the Taylor series expansion of $\chi(x)$ about the point $x = 0$ is obtained as

$$\chi(x) = r_e^{-2}(1 + x)^{-2} \approx \frac{1}{r_e^2} - \frac{2}{r_e^2}x + \frac{3}{r_e^2}x^2 + \ldots. \tag{A13}$$

Using equation (A13) in (A7) and equating the coefficients x^2, x and x^0 yields the following relations

$$d_0 + \varphi_0 d_1 + \theta_0 d_2 = \frac{1}{r_e^2}, \tag{A14}$$

$$(2\varphi_0\tanh a)d_1 + \theta_0(2\tanh a - \coth a)d_2 = \frac{2}{ar_e^2}, \tag{A15}$$

$$\varphi_0\left(3\tanh^2 a - 1\right)d_1 + \theta_0\left(3\tanh^2 a - \frac{5}{2}\right)d_2 = \frac{3}{a^2 r_e^2}, \tag{A16}$$

where $A = d_0$, $B = d_1$, and $C = d_2$. The solution of equation (A14)- (A16) gives

$$\begin{aligned} d_0 &= \frac{1}{r_e^2} - \frac{3\tanh a}{ar_e^2} + \frac{3}{a^2 r_e^2} \\ d_1 &= -\frac{(\cosh 2a - 11)\tanh a}{2ar_e^2} - \frac{3(\cosh 2a - 3)}{2a^2 r_e^2} \\ d_2 &= \frac{2\left(3\tanh^2 a - 1\right)\cosh a}{ar_e^2} - \frac{6\sinh a}{a^2 r_e^2} \end{aligned} \tag{A17}$$

References

[1] C. Eckart, The penetration of potential barrier by electrons, Phys. Rev. 35 (1930) 1303, https://doi.org/10.1103/PhysRev.35.1303.
[2] N. Rosen, P.M. Morse, On the vibrations of polyatomic molecules, Phys. Rev. 42 (1932) 210, https://doi.org/10.1103/PhysRev.42.210.
[3] L. Hulthén, Ark. Mat. Astron. Fys. A 28 (1942) 5.
[4] T. Tietz, Potential energy function for diatomic molecules, J. Chem. Phys. 38 (1963) 3036, https://doi.org/10.1063/1.1733648.
[5] D. Schiöberg, The energy eigenvalues of hyperbolical potential functions, Mol. Phys. 59 (1986) 1123, https://doi.org/10.1080/00268978600102631.
[6] Y.P. Varshni, Comparative study of potential energy functions for diatomic molecules, Rev. Mod. Phys. 29 (1957) 664, https://doi.org/10.1103/RevModPhys.29.664.
[7] C.S. Jia, Y.F. Diao, X.J. Liu, P.Q. Wang, J.Y. Liu, G.D. Zhang, Equivalence of the Wei potential model and Tietz potential model for diatomic molecules, J. Chem. Phys. 137 (2012), 014101, https://doi.org/10.1063/1.4731340.
[8] E.S. Eyube, G.G. Nyam, P.P. Notani, Improved q-deformed Scarf II oscillator, Phys. Scripta 96 (2021), 125017, https://doi.org/10.1088/1402-4896/ac2eff.
[9] M. Eshghi, R. Sever, S.M. Ikhdair, Thermal and optical properties of two molecular potentials, Eur. Phys. J. A 134 (2019) 155, https://doi.org/10.1140/epjp/i2019-12634-x.
[10] J.A. Kunc, F.J. Gordillo-Vázquez, Rotational-vibrational levels of diatomic molecules represented by the Tietz-Hua rotating oscillator, J. Phys. Chem. A 101 (1997) 1595, https://doi.org/10.1021/jp962817d.
[11] E.S. Eyube, P.P. Notani, M.M. Izam, Potential parameters and eigenspectra of improved Scarf II potential energy function for diatomic molecules, Mol. Phys. 120 (2022), e1979265, https://doi.org/10.1080/00268976.2021.1979265.
[12] P.Q. Wang, J.Y. Liu, L.H. Zhang, S.Y. Cao, C.S. Jia, Improved expressions for the Schiöberg potential energy models for diatomic molecules, J. Mol. Spectrosc. 278 (2012) 23, https://doi.org/10.1016/j.jms.2012.07.001.
[13] U.S. Okorie, A.N. Ikot, E.O. Chukwuocha, The improved deformed exponential-type potential energy model for N_2, NI, ScI and RbH diatomic molecules, Bull. Kor. Chem. Soc. 41 (2020) 609, https://doi.org/10.1002/bkcs.12039.
[14] C.S. Jia, L.H. Zhang, X.L. Peng, Improved Pöschl-Teller potential energy model for diatomic molecules, Int. J. Quant. Chem. 117 (2017), e25383, https://doi.org/10.1002/qua.25383.
[15] H. Yanar, A. Taş, M. Salti, O. Aydogdu, Ro-vibrational energies of CO molecule via improved generalized Pöschl-Teller potential and Pekeris-type approximation, Eur. Phys. J. A 135 (2020) 292, https://doi.org/10.1140/epjp/s13360-020-00297-9.
[16] H.R. Rastegar Sedehi, R. Khordad, Magnetocaloric effect, magnetic susceptibility and specific heat of tuned quantum dot/ring systems, Physica A 134 (2021), 114886, https://doi.org/10.1016/j.physe.2021.114886.
[17] E. Omugbe, O.E. Osafile, I.B. Okon, U.S. Okorie, K.O. Suleman, I.J. Njoku, A. Jahanshir, C.A. Onate, The influence of external magnetic and Aharonov-Bohm flux fields on bound states of the Klein-Gordon and Schrödinger equations via the SWKB approach, Eur. Phys. J. D 76 (2022) 177, https://doi.org/10.1140/epjd/s10053-022-00507-2.
[18] E.S. Eyube, P.P. Notani, D. Yabwa, E. Omugbe, C.A. Onate, I.B. Okon, G.G. Nyam, Y.Y. Jabil, M.M. Izam, Isobaric molar heat capacity model for the improved Tietz potential, Int. J. Quant. Chem. 123 (2023), e27040, https://doi.org/10.1002/qua.27040.
[19] R. Khordad, A. Ghanbari, Analytical calculations of thermodynamic functions of lithium dimer using modified Tietz and Badawi-Bessis-Bessis potentials, Comp. Theor. Chem. 1155 (2019) 1, https://doi.org/10.1016/j.comptc.2019.03.019.
[20] R. Khordad, H.R.R. Sedehi, M. Sharifzadeh, Susceptibility, entropy and specific heat of quantum rings in monolayer graphene: comparison between different entropy formalism, J. Comput. Electron. 21 (2022) 422, https://doi.org/10.1007/s10825-022-01857-1.
[21] Z.Z. Alisultanov, R.P. Meilanov, L.S. Paixão, M.S. Reis, Oscillating magnetocaloric effect in quantum nanoribbons, Physica A: Low-Dimens. Syst. Nanostructures 65 (2015) 44, https://doi.org/10.1016/j.physe.2014.08.012.
[22] Q.C. Ding, C.S. Jia, C.W. Wang, X.L. Peng, J.Y. Liu, L.H. Zhang, R. Jiang, S.Y. Zhu, H. Yuan, H.X. Tang, Unified non-fitting formulation representation of the thermodynamic properties for diatomic substances, J. Mol. Liq. 371 (2023), 121088, https://doi.org/10.1016/j.molliq.2022.121088.
[23] E.S. Eyube, G.G. Nyam, P.P. Notani, M.M. Izam, Y.Y. Jabil, Energy spectrum and magnetic properties of the Tietz oscillator in external magnetic and Aharonov-Bohm flux fields, Indian J. Phys. (2023), https://doi.org/10.1007/s12648-023-02811-y.
[24] E.S. Eyube, C.A. Onate, E. Omugbe, C.M. Nwabueze, Theoretical prediction of Gibbs free energy and specific heat capacity of gaseous molecules, Chem. Phys. 560 (2022), 111572, https://doi.org/10.1016/j.chemphys.2022.111572.
[25] R. Khordad, A. Ghanbari, Theoretical prediction of thermal properties of K_2 diatomic molecule using generalized Mobius square potential, Int. J. Thermophys. 42 (2021) 115, https://doi.org/10.1007/s10765-021-02865-2.
[26] D.C. Liang, R. Zeng, C.W. Wang, Q.C. Ding, L.S. Wei, X.L. Peng, J.Y. Liu, J. Yu, C.S. Jia, Prediction of thermodynamic properties of sulfur dioxide, J. Mol. Liq. 352 (2022), 118722, https://doi.org/10.1016/j.molliq.2022.118722.
[27] K.R. Purohit, R.H. Parmar, A.K. Rai, Solution of the modified Yukawa-Kratzer potential under influence of the external fields and its thermodynamic properties, J. Math. Chem. 60 (2022), https://doi.org/10.1007/s10910-022-01397-w, 1930.
[28] G.J. Rampho, A.N. Ikot, C.O. Edet, U.S. Okorie, S, Energy spectra and thermal properties of diatomic molecules in the presence of magnetic and AB fields with improved Kratzer potential, Mol. Phys. 110 (2020) (2020), e1821922, https://doi.org/10.1080/00268976.2020.1821922.
[29] S.H. Dong, W.H. Huang, P. Sedaghatnia, H. Hassanabadi, Exact solution of an exponential-type position dependent mass problem, Results Phys. 34 (2022), 105294, https://doi.org/10.1016/j.rinp.2022.105294.
[30] M. Eshghi, H. Mehraban, Study of a 2D charged particle confined by a magnetic and AB flux fields under the radial scalar power potential, Eur. Phys. J. A 132 (2017) 121, https://doi.org/10.1140/epjp/i2017-11379-x.
[31] S. Miraboutalebi, Solutions of Morse potential with position-dependent mass by Laplace transform, J. Theor. Appl. Phys. 10 (2016) 323, https://doi.org/10.1007/s40094-016-0232-x.
[32] R. Horchani, H. Al-Aamri, N. Al-Kindi, A.N. Ikot, U.S. Okorie, G.J. Rampho, H. Jelassi, Energy spectra and magnetic properties of diatomic molecules in the presence of magnetic and AB fields with the inversely quadratic Yukawa potential, Eur. Phys. J. D 75 (2021) 36, https://doi.org/10.1140/epjd/s10053-021-00038-2.
[33] C.O. Edet, P.O. Amadi, M.C. Onyeaju, U.S. Okorie, R. Sever, G.J. Rampho, H.Y. Abdullah, I.H. Salih, A.N. Ikot, Thermal properties and magnetic susceptibility of Hellmann potential in Aharonov-Bohm (AB) flux and magnetic fields at zero and finite temperatures, J. Low Temp. Phys. 202 (2021) 83, https://doi.org/10.1007/s10909-020-02533-z.
[34] A.N. Ikot, C.O. Edet, P.O. Amadi, U.S. Okorie, G.J. Rampho, H.Y. Abdulla, Thermodynamic properties of Aharanov–Bohm (AB) and magnetic fields with screened Kratzer potential, Eur. Phys. J. D 74 (2020) 159, https://doi.org/10.1140/epjd/e2020-10084-9.
[35] M. Eshghi, H. Mehraban, S.M. Ikhdair, Relativistic Killingbeck energy states under external magnetic fields, Eur. Phys. J. A 52 (2016) 201, https://doi.org/10.1140/epja/i2016-16201-4.
[36] C. Tezcan, R. Sever, Exact solutions of the Schrödinger equation with position-dependent effective mass via general point canonical transformation, J. Math. Chem. 42 (2007) (2006) 387, https://doi.org/10.1007/s10910-006-9109-6.
[37] B. Tang, C.S. Jia, Relativistic spinless rotation-vibrational energies of carbon monoxide, Eur. Phys. J. A 132 (2017) (2017) 375, https://doi.org/10.1140/epjp/i2017-11657-7.
[38] E.S. Eyube, Entropy and Gibbs free energy equations for the specialized Pöschl-Teller potential, Eur. Phys. J. A 137 (2022) 760, https://doi.org/10.1140/epjp/s13360-022-02931-0.
[39] M. Eshghi, R. Sever, S.M. Ikhdair, Energy states of the Hulthén plus Coulomb-like potential with position-dependent mass function in external magnetic fields, Chin. Phys. B 27 (2018), 020301, https://doi.org/10.1088/1674-1056/27/2/020301.
[40] A.N. Ikot, U.S. Okorie, G. Osobonye, P.O. Amadi, C.O. Edet, M.J. Sithole, G.J. Rampho, R. Sever, Superstatistics of Schrödinger equation with pseudo-harmonic potential in in external magnetic and Aharonov-Bohm fields, Heliyon 6 (2020), e03738, https://doi.org/10.1016/j.heliyon.2020.e03738.

[41] S. Faniandari, A. Suparmi, C. Cari, Study of thermomagnetic properties of diatomic particles using hyperbolic function position dependent mass under the external hyperbolic magnetic and AB force, Mol. Phys. 120 (2022), e2083712, https://doi.org/10.1080/00268976.2022.2083712.

[42] M. Eshghi, H. Mehraban, S.M. Ikhdair, Approximate energies and thermal properties of a position-dependent mass charged particle under external magnetic fields, Chin. Phys. B 26 (2017), 060302, https://doi.org/10.1088/1674-1056/26/6/060302.

[43] K.R. Purohit, R.H. Parmar, A.K. Rai, Bound state solution and thermodynamic properties of the screened cosine Kratzer potential under influence of the magnetic field and Aharanov-Bohm flux field, Ann. Phys. 424 (2021), 168335, https://doi.org/10.1016/j.aop.2020.168335.

[44] E.S. Eyube, J.B. Yerima, A.D. Ahmed, J-state solutions and thermodynamic properties of the Tietz oscillator, Phys. Scripta 96 (2021), 055001, https://doi.org/10.1088/1402-4896/abe3be.

[45] O. Mustafa, On the ro–vibrational energies for the lithium dimer; maximum-possible rotational levels, J. Phys. B Atom. Mol. Opt. Phys. 48 (2015), 065101, https://doi.org/10.1088/0953-4075/48/6/065101.

[46] E.S. Eyube, H. Samaila, I.B. Okon, P.U. Tanko, C.A. Onate, D. Yabwa, P.P. Notani, E. Omugbe, Energy levels of the improved Tietz oscillator in external magnetic and Aharonov-Bohm flux fields: the Pekeris approximation recipe, Eur. Phys. J. A 138 (2023) 251, https://doi.org/10.1140/epjp/s13360-023-03830-8.

[47] E.S. Eyube, P.U. Tanko, P.P. Notani, D. Yabwa, B.M. Bitrus, U. Wadata, H. Samaila, Analytical energy levels of the Schrödinger equation for the improved generalized Pöschl-Teller oscillator with magnetic vector potential coupling, Eur. Phys. J. D 77 (2023) 88, https://doi.org/10.1140/epjd/s10053-023-00666-w.

[48] E.S. Eyube, P.P. Notani, U. Wadata, S.D. Najoji, B.M. Bako, D. Yabwa, P.U. Tanko, Energy spectrum and zero-temperature magnetic functions of a position-dependent mass system in a Pöschl-Teller-type potential constrained by a vector magnetic potential field, Phys. Scripta 98 (2023), 095019, https://doi.org/10.1088/1402-4896/acedd8.

[49] V.G. Bagrov, D.M. Gitman, Exact Solution of Relativistic Wave Equations, Kluwa Academic, Dordrecht, 1990.

[50] E.S. Eyube, P.P. Notani, G.G. Nyam, Y.Y. Jabil, M.M. Izam, Pure vibrational state energies and statistical-mechanical models for the reparameterized Scarf oscillator, Front. Physiol. 11 (2023), 978347, https://doi.org/10.3389/fphy.2023.978347.

[51] E.N. Bogachek, U. Landman, Edge states, Aharonov-Bohm oscillations, and thermodynamic and spectral properties in a two-dimensional electron gas with an antidote, Phys. Rev. B 52 (1995), 14067, https://doi.org/10.1103/PhysRevB.52.14067.

[52] F.J.S. Ferreira, F.V. Prudente, Pekeris approximation - another perspective, Phys. Lett. 377 (2013) 3027, https://doi.org/10.1016/j.physleta.2013.09.028.

[53] F.J.S. Ferreira, V.B. Bezerra, Some remarks concerning the centrifugal term approximation, J. Math. Phys. 58 (2017), 102104, https://doi.org/10.1063/1.5008654.

[54] A. Bera, A. Ghosh, Analyzing magnetic susceptibility of impurity doped quantum dots in presence of noise, J. Magn. Magn Mater. 484 (2019) 391, https://doi.org/10.1016/j.jmmm.2019.04.005.

[55] M.L. Strekalov, An accurate closed-form expression for the partition function of Morse oscillators, Chem. Phys. Lett. 439 (2007) 209, https://doi.org/10.1016/j.cplett.2007.03.052.

[56] D. Li, F. Xie, L. Li, A. Lazoudis, A.M. Lyyra, New observation of the ^{6}Li^{7}Li, 3 $^{2}\Sigma_{g}^{+}$, 1 $^{3}\Delta_{g}$ and 2 $^{3}\Pi_{g}$ states and molecular constants with all $^{6}Li_{2}$, $^{7}Li_{2}$, and ^{6}Li^{7}Li data, J. Mol. Spectrosc. 246 (2007) 180, https://doi.org/10.1016/j.jms.2007.09.008.

[57] J. Heinze, U. Schühle, F. Engelke, C.D. Caldwell, D, Doppler-free polarization spectroscopy of the B $^{1}\Pi_{u}$ - X $^{1}\Sigma_{g}^{+}$ band system of K_2, J. Chem. Phys. 95 (1991) (1987) 4168, https://doi.org/10.1063/1.453591.

[58] W.J. Balfour, A.E. Douglas, Absorption spectrum of the Mg_2 molecule, Can. J. Phys. 48 (1970) 901, https://doi.org/10.1139/p70-116.

[59] S. Zeid, N. El-Kork, M. Korek, Electronic structure with the calculation of the Rovibrational, and dipole moments of the electronic states of the NaBr and KBr molecules, Chem. Phys. 517 (2019) 36, https://doi.org/10.1016/j.chemphys.2018.09.037.

[60] D. Shokov, M. Murakami, J.J. Honrubia, Laser scaling for generation of megatesla magnetic fields by microtube implosions, High Power Laser Sci. Eng. 9 (2021) e56, https://doi.org/10.1017/hpl.2021.46.

[61] A. Kumar, S.M. Yusuf, The phenomenon of negative magnetization and its implications, Phys. Rep. 55 (2015) (2015) 1, https://doi.org/10.1016/j.physrep.2014.10.003.